Available online at www.sciencedirect.com
SCIENCE DIRECT®
International Journal of Heat and Mass Transfer 48 (2005) 4667–4683
International Journal of HEAT and MASS TRANSFER
www.elsevier.com/locate/ijhmt

Non-linear analyses of flow boiling in microchannels

R. Mosdorf [a,*], Ping Cheng [c,1], H.Y. Wu [c,1], M. Shoji [b,2]

[a] Faculty of Computer Science, Bialystok University of Technology, 15-351 Bialystok, ul. Wiejska, Poland
[b] National Institute of Advanced Industrial Science and Technology (AIST Tsukuba), Namiki 1-2-1, Tsukuba, Ibaraki 305-8564, Japan
[c] School of Mechanical and Power Engineering, Shanghai Jiaotong University, Shanghai 200030, PR China

Abstract

Recently, four unstable boiling cases with different fluctuating amplitudes were observed in parallel silicon microchannels having a hydraulic diameter of 186 μm. These were: the liquid/two-phase alternating flow (LTAF) at two different heat fluxes, the continuous two-phase flow (CTF) at medium heat flux and medium mass flux, and the liquid/two-phase/vapor alternating flow (LTVAF) at high heat flux and low mass flux. In this paper, data of these unstable boiling cases are analyzed using the following methods: correlation coefficient, attractor reconstruction, correlation dimension and largest Lyapunov exponent. The processes responsible for appearance of chaotic oscillations in microchannels, such as nucleation, stability of bubbly flow, vapour core stability and vapour-phase flow stability, are discussed. It is shown that under certain conditions, the microchannels system works as a thermal oscillator. It was found that heat supplied to the microchannels increases the heating surface temperature while the appearance of the two-phase flow inside the channels decreases the heating surface temperature. The mechanism involving an increase in heating surface temperature is supported by phenomena of blocking the liquid flow in microchannels by the two-phase flow.

Keywords: Boiling heat transfer; Microchannels; Instability; Nonlinear analysis

1. Introduction

It is well known that boiling instabilities occur in macrosystems, and many mechanisms can lead to such unstable behaviors. Depending on the mechanism, various types of static and dynamic instabilities (such as nucleation instabilities, flow pattern instabilities, Ledinegg instabilities, thermal oscillations, density-wave type oscillations, pressure-drop type oscillations) may arise [1–6]. Early works on boiling in microchannels and minichannels, however, were focused on the stable mode of boiling heat transfer process [7–10]. Recently, some investigators [11–13] observed boiling instability in smaller silicon microchannels. Most recently, Wu and Cheng [14–18] reported large-amplitude oscillations of temperature and pressures in silicon microchannels when the wall heat flux was increased beyond the incipient boiling point. They also observed that two-phase flow and single-phase liquid flow appeared alternatively with time in the microchannel under certain conditions.

* Corresponding author. Tel.: +48 85 7422 041; fax: +48 85 7422 393.
E-mail addresses: mosdorf@ii.pb.bialystok.pl (R. Mosdorf), pingcheng@sjtu.edu.cn (P. Cheng), whysrj@sjtu.edu.cn (H.Y. Wu), shoji.m@aist.go.jp (M. Shoji).
[1] Tel.: +86 21 6293 3154; fax: +86 21 6293 3107.
[2] Tel.: +81 29 861 7053; fax: +81 29 861 7053/7275.

0017-9310/$ - see front matter © 2005 Elsevier Ltd. All rights reserved.
doi:10.1016/j.ijheatmasstransfer.2005.01.046

Nomenclature

Cov	covariation function
C	correlation coefficient
D	correlation dimension
d	distance in phase space
L'	distance between the trajectories
L	largest Lyapunov coefficient, bit/s
m	mass flux, g/cm^2 s
N	number of samples
p	pressure, Pa
P	probability
q	heat flux, W/cm^2
T	temperature, °C
t	time, s

Greek symbols

λ	largest Lyapunov exponent, bit/s
τ	time interval
σ	standard deviation
Θ	Heaviside's step function

Subscripts

i, j	sample number
in	inlet
o	outlet
wi	heating surface

In this paper, nonlinear analysis methods, such as the attractor reconstruction, correlation dimension and largest Lyapunov exponent, are used to study the behaviour of unstable boiling cases in microchannels as observed by Wu and Cheng [18]. The results of this analysis show that the appearance of two-phase flow in microchannel controls the mass flux and decrease of heating surface temperature. The processes of nucleation, stability of bubbly flow, vapour core stability and vapour-phase flow stability, which are responsible for the appearance of chaotic oscillations in microchannels, are discussed.

2. Wu and Cheng's experimental data

As discussed by Wu and Cheng [14,18], the experimental setup consisted of a constant-pressure tank, a valve regulator, a filter, a flow meter, a test section, and a collecting container. The deionized and degassed water in the pressure tank, being pushed by the compressed nitrogen gas, flowed successively through a valve, a filter, a flow meter, and then to the test section which was heated by a film heater. After the water was heated in the test section, it was collected in a container with a small hole vented to the atmosphere. The container was placed on a precision electronic balance, and the average mass flux of water was determined by calculating the mass increment per unit time. The test section, consisting of the eight parallel silicon microchannels (having identical trapezoidal cross-section with a hydraulic diameter of 186 μm and a length of 30 mm) etched on a ⟨1 0 0⟩ silicon wafer, is shown in Fig. 1a. The microchannels were sealed from the top by a thin pyrex glass plate which allowed visualization of the boiling phenomena occurring inside the microchannels. A microscope and a high-speed video recording system, located above the microchannels, were used for the visualization study. Two type-T thermocouples, having a diameter of 0.25 mm and a response time of 0.2 s, were used to measure water temperatures at the inlet and outlet of the microchannels (T_{in}, T_o). The wall temperatures ($T_{w1}, T_{w2}, T_{w3}, T_{w4}, T_{w5}$) were measured by five type-T thermocouples, having a diameter of 0.1 mm and a response time of 0.1 s. The longitudinal locations of these thermocouples are shown in Fig. 1b.

As pointed out in the previous paper [18], when the heat flux was at a relatively low level and the flow everywhere in the microchannels was still in single phase, all of temperature, pressure, and mass flux data remained constant with time. However, as the heat flux was gradually increased (with corresponding decrease in mass flux while all other conditions remained unchanged) and the water temperature near the outlet of the microchannel reached the saturated condition, some bubbles began to appear near channel's outlets, and this state is usually referred to as the incipient boiling. At the incipient boiling condition, small temporal variations of temperatures, pressures, and mass flux were observed. As the heat flux was increased further, while other conditions in the experimental system remained unchanged, boiling occurred rapidly everywhere in all eight microchannels, and four unstable boiling modes were observed. These unstable boiling modes were: liquid/two-phase alternating flow (Cases 1a and 1b), continuous two-phase flow (Case 2), and liquid/two-phase/vapor alternating flow (Case 3). Simultaneously, oscillations of wall and water temperatures, pressures, and mass flux, were measured.

Fig. 2 shows the temporal changes of inlet and outlet fluid temperatures (T_{in}, T_o), and heating surface temperatures (T_{w1}, T_{w5}) as well as inlet liquid pressure (p_{in}) at different heat and mass fluxes. Fig. 2a shows the temporal variations of temperatures and inlet pressure for the

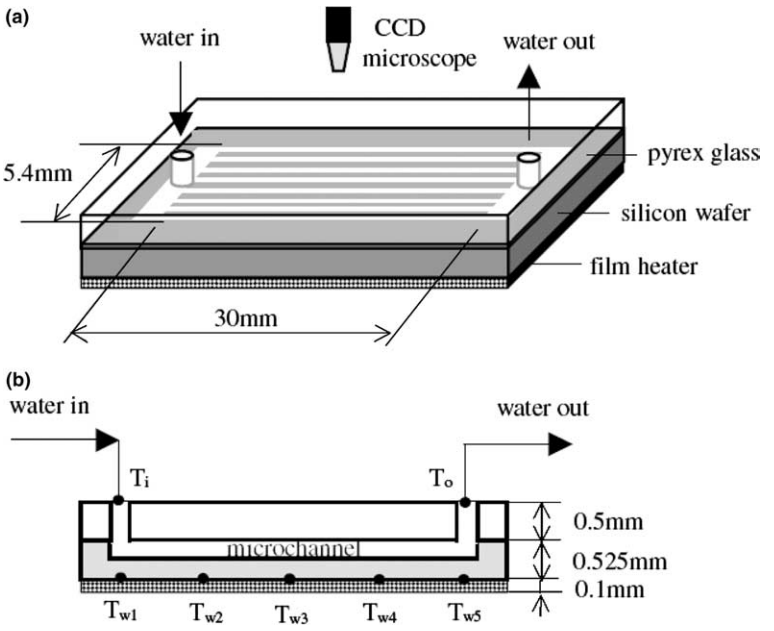

Fig. 1. Test section.

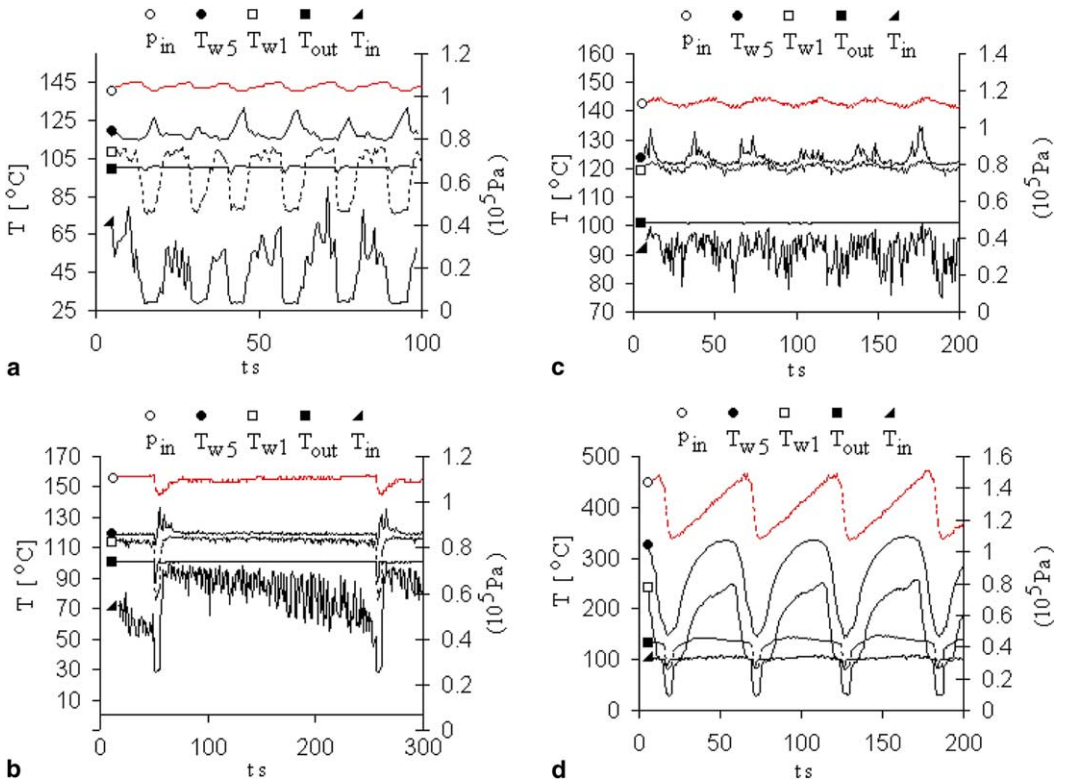

Fig. 2. Temporal variations of temperatures and pressure at different heat flux and mass flux. (a) Liquid/two-phase alternating flow: $q = 13.5$ W/cm^2 and $m = 14.6$ g/cm^2 s (Case 1a), (b) liquid/two-phase alternating flow: $q = 16.6$ W/cm^2 and $m = 12.7$ g/cm^2 s (Case 1b), (c) continuous two-phase flow: $q = 18.8$ W/cm^2 and $m = 11.9$ g/cm^2 s (Case 2) and (d) liquid/two-phase/vapor alternating flow: $q = 22.6$ W/cm^2 and $m = 11.2$ g/cm^2 s (Case 3).

liquid/two-phase alternating flow (Case 1a) in the microchannel when the heat flux was increased to 13.5 W/cm^2 and the corresponding mass flux was 14.6 g/cm^2 s. In this mode with a period of 15.4 s, it began with a single phase that lasted for 5.4 s, and it changed to bubbly flow for 10 s before it suddenly changed back to the liquid phase again. As the experiment continued, this alternation from single-phase liquid flow to two-phase flow repeated itself. The visualization study also showed that bubbly flow was the dominant flow pattern during the two-phase flow period at this heat flux and mass flux.

Fig. 2b shows the temporal variations of temperatures and inlet pressure for Case 1b when the heat flux was increased to 16.6 W/cm^2 and the corresponding average mass flux was decreased to 12.7 g/cm^2 s. The boiling flow pattern is similar to Case 1a, i.e., liquid/two-phase alternating flow in which liquid phase and bubbly flow appear. The period of Case 1b is much longer than Case 1a. During a cycle, about 97.5% of time was occupied by the two-phase flow period whereas only 2.5% time was occupied by the single-phase liquid flow period.

When the heat flux was further increased to 18.8 W/cm^2 and the corresponding average mass flux was decreased to 11.9 g/cm^2 s (Case 2), the liquid-phase period disappeared completely, and a new boiling mode: the continuous two-phase flow was observed in the parallel microchannels (Fig. 2c). For this case, many bubbles generated from the bottom corners of the microchannels, and there appeared a vapor core (due to the coalescence of large bubbles) moving in the middle of microchannels.

As the heat flux was further increased to 22.6 W/cm^2 and the corresponding mass flux was decreased to 11.2 g/cm^2 s (Case 3), another new boiling instability mode: liquid/two-phase/vapor alternating flow, was observed inside the parallel microchannels (Fig. 2d). This unstable boiling mode, observed at the mid-length of the microchannels, can be described as follows: after a 4 s liquid-phase period, it changed to the two-phase flow that lasted about 10 s, and then it further changed to a superheated vapor flow. The superheated vapor flow lasted about 23 s, and was followed by another two-phase flow period that lasted about 16 s. At the end of this two-phase flow period, a new cycle starting from liquid-phase flow began. The total period was approximately 53 s.

3. Data analysis

3.1. Correlation coefficients

In this section, we will study the correlation between temperatures of heating surface as well as the temperature and pressure of the fluid measured by Wu and Cheng [18] under different heat fluxes and mass fluxes conditions. The results of the present analysis can provide information about dynamic behaviors of flow boiling in microchannels under these conditions. The temperature measurements at points T_{w1}, T_{w2}, T_{w3}, T_{w4}, T_{w5} show the dynamics of local heat transfer processes between boiling liquid and heating surface. The temperatures of T_{in}, and T_o, measure an average result of heat and mass transfer inside the microchannels. Identification of correlation between the time series can be calculated using the correlation coefficient, which is calculated as follows [19]:

$$C = \frac{\mathrm{Cov}(T_i, T_j)}{\sigma_{T_i}\sigma_{T_j}} \tag{1}$$

where T_i and T_j are time series of temperatures measured at different points; σ_{T_i} and σ_{T_j} are the standard deviations. Note that when $|C|$ is close to 1, time series T_i and T_j are correlated. When the large and low values in both series appear at the same time, then $C > 0$; but when large values in first series meet low values in other series, then $C < 0$. When C is close to zero, then the time series T_i and T_j are not correlated.

As discussed in the previous paragraph, Wu and Cheng [18] have observed the following flow patterns in microchannels under different conditions: liquid-phase flow, bubbly flow, vapor core flow and vapor-phase flow. Each flow pattern in microchannel system existed at some ranges of parameters such as heating surface temperature, inlet liquid pressure, heat and mass fluxes. When any of parameters exceeds the range of flow pattern occurrence, then the flow pattern in microchannels changes. The existing flow pattern disappears and a new one appears. We will say that the existing flow pattern becomes unstable and the new structure becomes stable. When we observe in microchannels the process in which the subsequent changes of flow pattern appears, this means that all observed flow patterns become alternately stable and unstable during the process. The stability of flow pattern depends on temporal variations of such parameters as: temperatures of heating surface and liquid, mass and heat fluxes and liquid pressure. The temporal variations of liquid and wall temperature in Fig. 2 illustrate that temporal changes of outlet liquid temperature was relatively low in comparison with other temperature changes. In fact, the amplitude and data resolution of outlet liquid temperature is too small for carrying out dynamic analysis. For this reason, only the temperatures of inlet liquid and heating surface, as well as inlet pressure will be analyzed in this paper.

The values of correlation coefficient between the time series of temperature T_{w1} and T_{w2}, T_{w3}, T_{w4}, T_{w5}, for four cases under consideration are presented in Fig. 3 where the horizontal axis indicates measurement points. For example, the point '1–3' on the horizontal axis means that the correlation coefficient between T_{w1} and

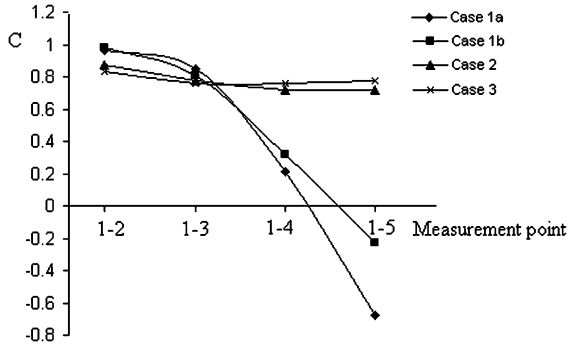

Fig. 3. Correlation coefficient between the different temperature series at different heat and mass fluxes.

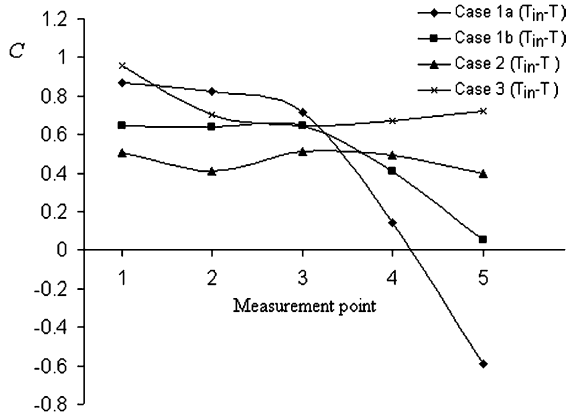

Fig. 4. Correlation coefficient between inlet liquid temperature and heating surface temperature at different heat and mass fluxes. (a) Liquid/two-phase alternating flow: $q = 13.5$ W/cm^2 and $m = 14.6$ g/cm^2 s (Case 1a), (b) liquid/two-phase alternating flow: $q = 16.6$ W/cm^2 and $m = 12.7$ g/cm^2 s (Case 1b), (c) continuous two-phase flow: $q = 18.8$ W/cm^2 and $m = 11.9$ g/cm^2 s (Case 2) and (d) liquid/two-phase/vapor alternating flow: $q = 22.6$ W/cm^2 and $m = 11.2$ g/cm^2 s (Case 3).

T_{w3} was calculated. The correlation coefficient between inlet liquid temperatures T_{in} and wall temperatures T_{w1}, T_{w2}, T_{w3}, T_{w4}, T_{w5}, are presented in Fig. 4 where the horizontal axis indicates measurement points. For example, '3' means that the correlation between the T_{in}, and T_{w3} was calculated. As mentioned earlier, positive values of correlation coefficients in Figs. 3 and 4 mean that the two temperature time series under consideration are correlated in such a way that maximums of temperatures in both series appear at the same time. Negative values of correlation coefficients mean that the two temperature time series under consideration are correlated in such a way that the minimum value of temperature occurs in the first series and at the same time the maximum value occurs in the second series. When values of correlation coefficient approach to zero, then the two time series under consideration are not correlated. This occurs in Cases 1a, 1b near the end of the microchannels.

Fig. 3 shows that surface temperature changes at the entrance region, i.e., T_{w1}, T_{w2}, T_{w3} for Cases 1a and 1b are correlated in the same way. However, near the outlet of the microchannels, i.e., T_{w5}, the value of the correlation coefficient is negative, i.e., T_{w5} is not correlated with T_{w1} in the same way. On the other hand, for Cases 2 and 3, all of the surface temperatures are correlated in the same way.

Similarly, Fig. 4 shows the correlation coefficient between the inlet water temperature and the surface temperatures. All of the surfaces temperatures in Cases 2 and 3 are correlated in the same way with the inlet water temperature. However, although surfaces temperatures at measurement points T_{w1}, T_{w2}, T_{w3} in Cases 1a and 1b are correlated in the same way, qualitative differences between temperature change characteristics occurred near the end of the microchannel in these cases.

3.2. Attractor reconstruction

Behaviors of a chaotic system can also be analyzed based on the trajectories of the system in the phase space [19,21,22]. The analysis begins with reconstruction of the attractor. This reconstruction in certain embedding dimension can be carried out using the stroboscope coordination [19]. In this method, co-ordinates of attractor points are calculated based on the subsequent samples between which the distance is equal to time delay τ [19]. The image of the attractor in D-dimensional space depends on the magnitude τ. An example of attractor reconstruction for different delay-time τ is shown in Fig. 5. When the delay-time is too small, the attractor gets flattened (as shown in Fig. 5a) which makes the further analysis of its structure impossible. When the delay-time τ is too large (Fig. 5c), the attractor becomes too complex, and further analysis would give wrong information about the dynamic properties of the system under consideration [19]. Therefore, the selection of delay-time value is of great significance in the analysis of the attractor properties. However, the selection of delay-time cannot be done automatically and must be checked after each calculation manually. In this study, we chose the proper value of τ using the special software [21] that allows us to observe the animation of 3D attractor rotation. This software enabled us to choose manually the proper value of time delay. For the cases under consideration, when we increase the time-delay, the trajectories of attractor start to fill the torus, as shown in Fig. 5d. When the delay-time is increased further, the torus caves in, as is shown in Fig. 5c. The proper value of τ is chosen for which the torus diameter would reach the maximum value. The trajectories of system reconstructed in state-space (p_{in}, T_{in}, T_w) are also located inside some torus, as will be shown in

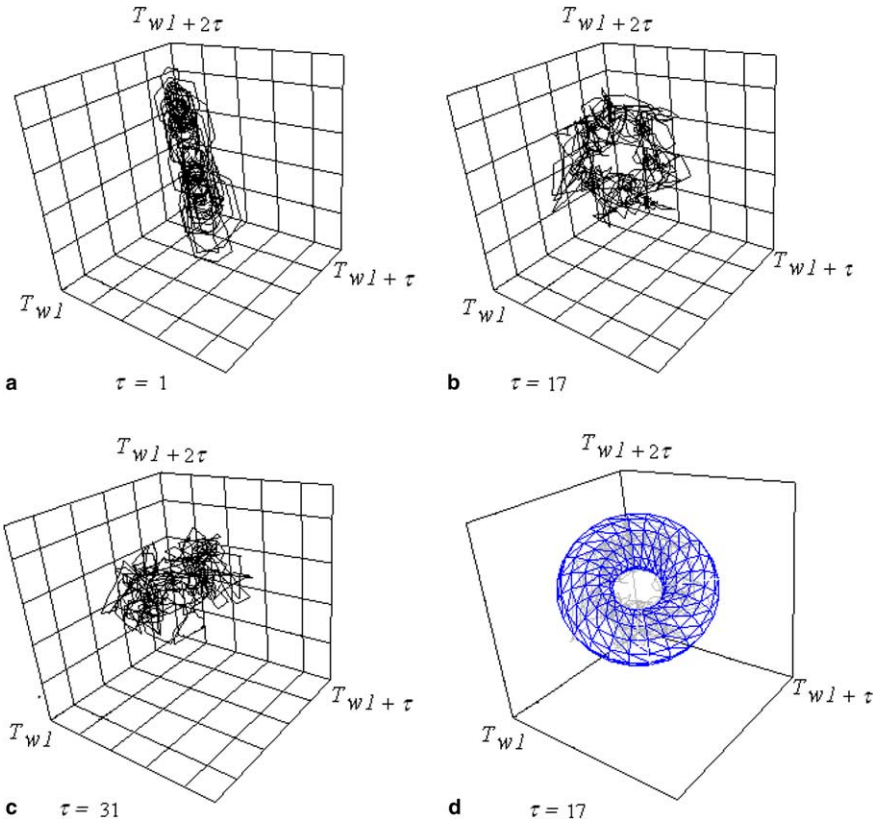

Fig. 5. 3D attractor reconstruction from temperature T_{w1} in continuous two-phase flow: $q = 18.8$ W/cm^2 and $m = 11.9$ g/cm^2 s (Case 2) for different time delay τ. (a) $\tau = 1$ samples, (b) $\tau = 17$ samples, (c) $\tau = 31$ samples and (d) schematic drawing of torus containing trajectories for $\tau = 17$ samples.

the subsequent part of the paper. This proves that the method of choosing delay-time in the paper is appropriate.

The attractors reconstruction from temperature T_{w1} for different heat fluxes are shown in Fig. 6 while the attractors reconstruction from inlet pressure fluctuation at different heat and mass fluxes are shown in Fig. 7. Coordinates of points of attractors are created from single time series (T_{w1} or p_{in}) using the delay-time method. Therefore, the coordinates of attractor points in embedding space are T_i, $T_{i+1\tau}$, $T_{i+2\tau}$, and p_i, $p_{i+1\tau}$, $p_{i+2\tau}$ respectively. Black lines in Figs. 6 and 7 connect the subsequent points of attractors. Reconstruction of attractors from shorter time series can be used to identify which parts of attractors and measured data are adequate. When we know which processes are responsible for creation the parts of measured data, then we can identify parts of attractors corresponding to these processes. In Figs. 6 and 7, some areas of attractors corresponding to certain processes are marked approximately with grey circular shapes. This is because the shape of attractor is complex (such as those in Fig. 6c and Fig. 7c for Case 2), and the identification of points of attractor created by these processes is difficult. Note that coordinates of attractors have no physical meaning, but they can be used to reconstruct the multidimensional system dynamic from the single time series (for example from temperature measurement at a single measurement point). According to the Takens theorem [19], however, the topological properties of attractors reconstructed in this artificial space correspond to topological properties of attractors created in the physical state-space, where its coordinates correspond to physical parameters such as: temperature, pressure, heat flux, mass flux, etc. Values on each axis in Figs. 6 and 7 represent the minimum and maximum values of investigated time series. It can be seen that amplitudes of temperature and pressure changes are different in the four cases under consideration. The largest amplitude of temperature and pressure changes appears in Case 2 (Figs. 6c and 7c) and the minimum amplitude of temperature changes appears in Case 3 (Fig. 6d), but the minimum amplitude of inlet pressure changes appears in Case 3 (Fig. 7d). The highest temperature of T_{w1} was reached in Case 3, which was

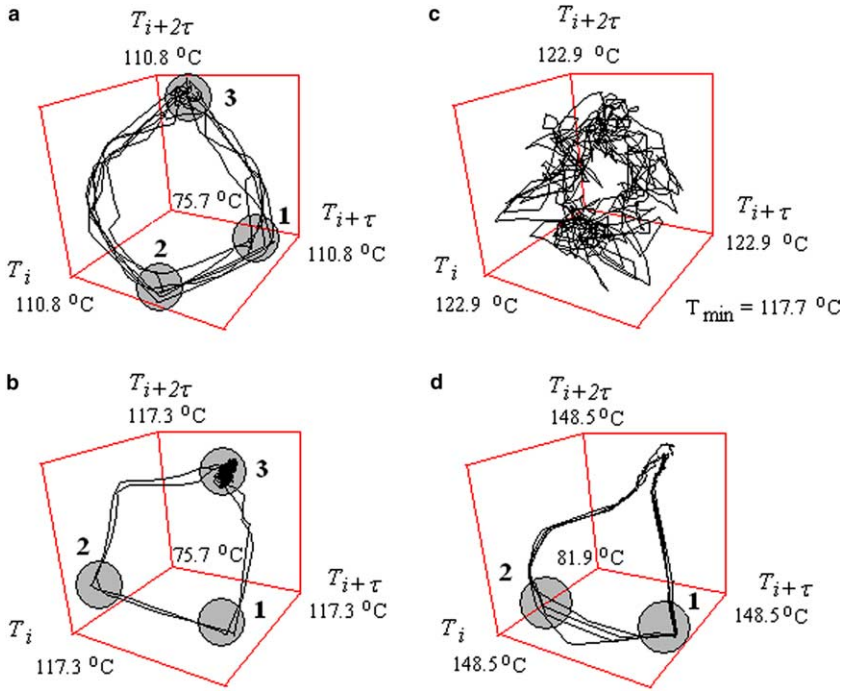

Fig. 6. Attractor reconstruction from T_{w1} at different heat and mass fluxes. (a) Liquid/two-phase alternating flow: $q = 13.5$ W/cm^2 and $m = 14.6$ g/cm^2 s, $\tau = 5.9$ s (Case 1a), 1—part of embedding space containing the points created by temperature changes during the nucleation disappearance, 2—part of embedding space containing the points created during the beginning of boiling, 3—part of embedding space containing the points created from temperature changes during the two-phase flow, (b) liquid/two-phase alternating flow: $q = 16.6$ W/cm^2 and $m = 12.7$ g/cm^2 s, $\tau = 5.9$ s (Case 1b), 1—part of embedding space containing the points created by temperature changes during the nucleation disappearance, 2—part of embedding space containing the points created during the beginning of boiling, 3—part of embedding space containing the points created from temperature changes during the two-phase flow, (c) continuous two-phase flow: $q = 18.8$ W/cm^2 and $m = 11.9$ g/cm^2 s, $\tau = 12.9$ s (Case 2) and (d) liquid/two-phase/vapor alternating flow: $q = 22.6$ W/cm^2 and $m = 11.2$ g/cm^2 s, $\tau = 5.6$ s (Case 3), 1—part of embedding space containing the points created by temperature changes during the nucleation disappearance, 2—part of embedding space containing the points created during the beginning of boiling.

equal to 148.5 °C (Fig. 6d). The maximum temperature of heating surface was the lowest in Case 1a, which was equal to 110.8 °C (Fig. 6a). The minimum value of heating surface temperature was reached in Cases 1a and 1b, which was equal to 75.7 °C (Fig. 6a and b). Minimum temperature of heating surface was the highest in Case 3 which was equal to 81.9 °C (Fig. 6d). The lowest inlet pressure was observed in Fig. 7a and b for Cases 1a and 1b, which was equal to 103 kPa.

Note that the shape of the attractor shows complexity of the system. In general, the trajectories of attractors are located inside the torus in 3D space for all cases under consideration. The system is more predictable when the trajectories lie close to each other such as in Case 3 (Figs. 6d and 7d) and more chaotic when locations of trajectories vary, such as in Case 2 (Figs. 6c and 7c). The points on attractor can be placed evenly in all parts of attractor (such as in Case 3, Fig. 6d) or unevenly, such as in Case 1b, where a large number of points are located in the area assigned by number '3' in Fig. 6b.

Because the three system parameters (temperature and pressure of liquid and heating surface temperature), were measured in Wu and Cheng's experiment, therefore, we can reconstruct the trajectory of the system in the state-space (T_{in}, p_{in}, T_w) where T_w is an average temperature of heating surface. The trajectories are presented in Fig. 8 where the arrows indicate the direction of changes in time. These directions are the same in all four cases under consideration. The trajectories are located inside the torus like trajectories obtained using the delay time method. The trajectories reconstructed in Fig. 8 can be used to explain the appearance of oscillations in the four cases under consideration as follows:

Cycles start from point "1" (Fig. 8) when heat was supplied to the system, where the temperature of the heating surface began to increase and two-phase flow began to appear in the microchannel. The appearance of

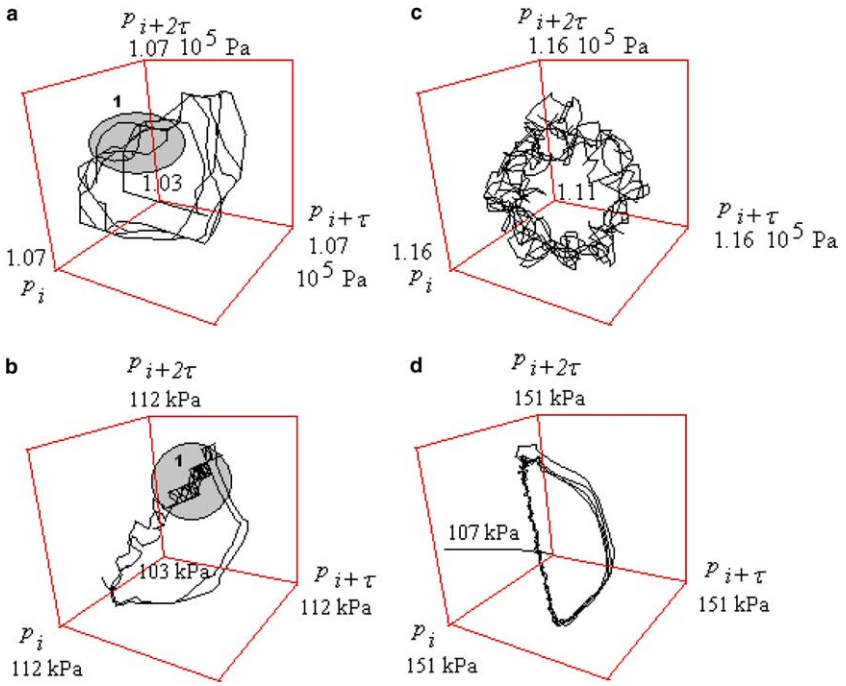

Fig. 7. Attractor reconstruction from p_i at different heat and mass fluxes. (a) Liquid/two-phase alternating flow: $q = 13.5$ W/cm^2 and $m = 14.6$ g/cm^2 s, $\tau = 5.9$ s (Case 1a), 1—part of embedding space containing the points created by pressure fluctuation during the two-phase flow period, (b) liquid/two-phase alternating flow: $q = 16.6$ W/cm^2 and $m = 12.7$ g/cm^2 s, $\tau = 5.9$ s (Case 1b), 1—part of embedding space containing the points created by pressure fluctuation during the two-phase flow period, (c) continuous two-phase flow: $q = 18.8$ W/cm^2 and $m = 11.9$ g/cm^2 s, $\tau = 12.9$ s (Case 2) and (d) liquid/two-phase/vapor alternating flow: $q = 22.6$ W/cm^2 and $m = 11.2$ g/cm^2 s, $\tau = 5.6$ s (Case 3).

the two-phase flow inside the microchannels blocked water flowing into the microchannel, and therefore the mass flux decreased. As a result, water was heated up in the inlet of the microchannels. During the boiling inside the microchanels the inlet water pressure increases and the process reached the point "2" (Fig. 8). The boiling inside the microchannels led to a decrease in the heating surface temperature, and consequently the bubbles stopped blocking the microchannel and inlet pressure decreased. The process reached again the point "1" (Fig. 8) and the cycle repeated itself.

3.3. Correlation dimensions

The trajectories of the chaotic system in the phase space do not form any single geometrical object such as circle or torus, but form objects called the strange attractors [19] of the structure resembling a fractal. One of the essential characteristics of fractals is their dimension. For experimental data, the correlation dimension D is defined by the following expression [19,20]:

$$D = \lim_{d\to 0} \frac{1}{\ln d} \ln \sum_i P_i \tag{2a}$$

where

$$\sum_i P_i \approx \lim_{N\to\infty} \frac{1}{N^2} \sum_{i,j} \Theta(d - |T_i - T_j|) \tag{2b}$$

with Θ being the Heaviside's step function that determines the number of attractor's point pairs of the distance shorter than d. Correlation dimension of the attractors created by the dynamic system can be used to identify the number of the system freedom degrees. The number of independent variables controlling the behaviours of the system is a lowest integer number greater than correlation dimension. Correlation dimensions for p_{in}, T_{in}, T_{wi} can be calculated based on Eq. (2) and these values are listed in Table 1.

When the values of correlation dimension obtained from T_{in} and p_{in} are close to each other (such as in Cases 1a, 1b, 3, see Table 1), then we can conclude that changes of T_{in} and p_{in} are controlled by the same set of physical parameters. In Case 2 the correlation dimension obtained from the T_{in} and p_{in} differ, which means that the sets of independent physical parameters describing the changes of T_{in} and p_{in} differ as well.

In Case 3 (Fig. 8d) trajectories in subsequent periods lie close with each other. In this case, only the process duration time, measured from the beginning of the cycle,

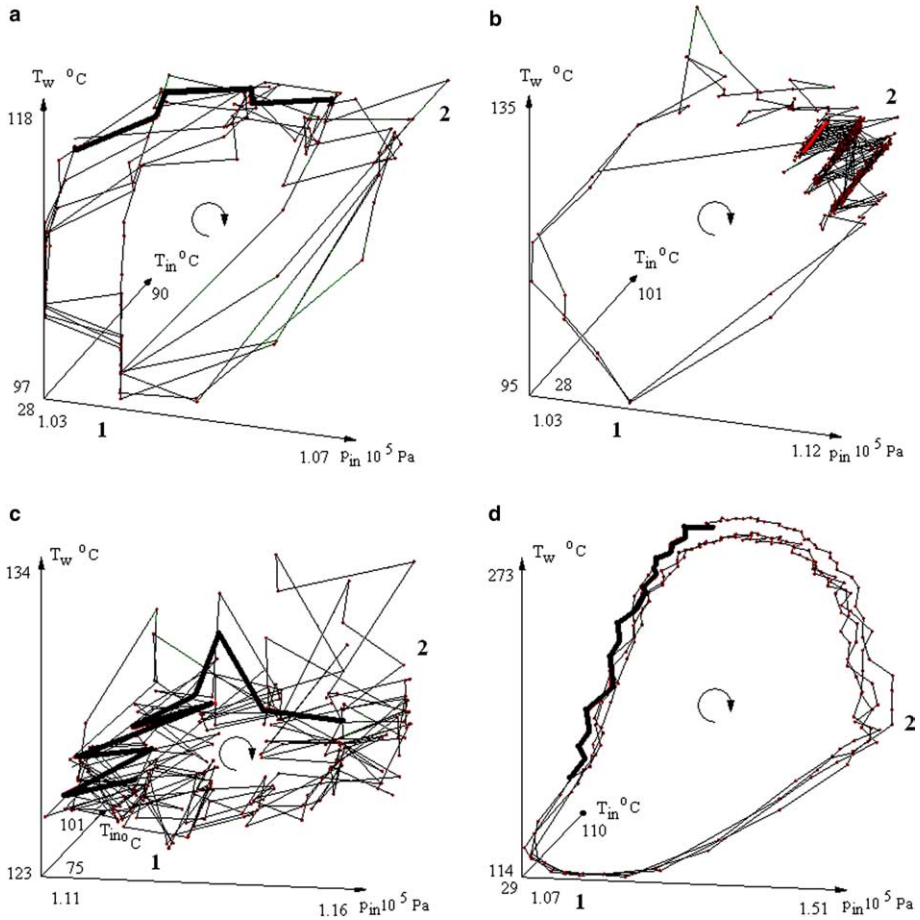

Fig. 8. Trajectories of oscillations in space (p_i, T_{w2}, T_{in}) at different heat and mass fluxes (arrows indicate the direction of time). (a) liquid/two-phase alternating flow: $q = 13.5$ W/cm^2 and $m = 14.6$ g/cm^2 s (Case 1a), (b) liquid/two-phase alternating flow: $q = 16.6$ W/cm^2 and $m = 12.7$ g/cm^2 s (Case 1b), (c) continuous two-phase flow: $q = 18.8$ W/cm^2 and $m = 11.9$ g/cm^2 s (Case 2), (d) liquid/two-phase/vapor alternating flow: $q = 22.6$ W/cm^2 and $m = 11.2$ g/cm^2 s (Case 3).

Table 1
Results of nonlinear analysis and experimental data for four boiling cases under consideration

	Case 1a	Case 1b	Case 2	Case 3
Heat flux, q	13.5 W/cm^2	16.6 W/cm^2	18.8 W/cm^2	22.6 W/cm^2
Mass flux, m	14.6 g/cm^2 s	12.7 g/cm^2 s	11.9 g/cm^2 s	11.2 g/cm^2 s
Oscillation period	15.4 s	202 s	32 s	53 s
Liquid period	5.4 s	5 s	0	4 s
Two-phase period	10.0 s	197 s	32 s	10 s/16 s
Vapour-phase period	0	0	0	23 s
Average temperature of heating surface	111 °C	120.9 °C	126.2 °C	212.3 °C
Average correlation dimension from heating surface temperature	$1.99^{+0.26}_{-0.18}$	$4.64^{+0.86}_{-0.54}$	$4.2^{+0.49}_{-0.7}$	$1.3^{+0.09}_{-0.09}$
Correlation dimension from p_{in}	2.25	5.5	4.2	1
Correlation dimension from T_{in}	2.25	5.2	6	1.1
Average Lyapunov exponent from the heating surface temperature [bit/s]	$0.254^{+0.036}_{-0.024}$	$0.046^{+0.036}_{-0.016}$	$0.126^{+0.064}_{-0.046}$	$0.054^{+0.076}_{-0.034}$
Lyapunov exponent from p_{in} [bit/s]	0.26	0.08	0.2	0.09
Lyapunov exponent from T_{in} [bit/s]	0.3	0.06	0.36	0.09
Average time of loss of stability	3.9 s 1/4 cycle	21.6 s 1/9 cycle	7.9 s 1/4 cycle	18.5 s 1/3 cycle

is necessary to describe the state of system, i.e., only one parameter is necessary to describe the system behavior. Therefore, the correlation dimension of the system in Case 3 is close to 1, and the system behaviour can be identified as close to periodical. In the other cases, the location of trajectories are more complicated, therefore the system behaviour can be identified as chaotic.

3.4. Lyapunov exponents

One of the quantities determining whether the behaviour of the dynamic system is chaotic is Lyapunov exponents [19]. From the measured data, it is possible to determine the value of the largest Lyapunov exponent. A positive value of the largest Lyapunov exponent indicates that deterministic chaos appear in the system under consideration. In this case, on the attractor immersed in D dimensional space two points situated at a distance of at least one orbiting period one from another, have been selected. The distance between these points is $L(t_j)$. The distance of the selected points after the passage of some evolution time has been calculated and defined as $L'(t_{j+1})$. A computer algorithm for calculation of the largest Lyapunov exponent has been proposed by Wolf [20], who gave the following formula to calculate the largest Lyapunov exponent

$$\lambda = \frac{1}{t}\sum_{j=1}^{m}\log_2\left[\frac{L'(t_{j+1})}{L(t_j)}\right] \tag{3}$$

where L is the distance between two points of attractor, m is number of tested point pairs, and t is the time of evolution. The long time memory can be calculated as $1/\lambda$. This time corresponds with average time in which the process of stability loss occurs. The largest Lyapunov exponent can be calculated for p_{in}, T_{in}, T_{wi} based on Eq. (3) and these values are listed in Table 1.

The appearance of deterministic chaos in cases under consideration is confirmed by positive value of largest Lyapunov exponent (see Table 1). The value of the largest Lyapunov exponent determines the rate of exponential divergence of the trajectory, and in the same way it determines the average time of stability loss in the system. Note that the average liquid velocity inside the microchannels in the four cases under consideration were: 15.2 cm/s, 13.3 cm/s, 12.4 cm/s, 11.7 cm/s in Cases 1a, 1b, 2 and 3 respectively. These average liquid velocities were calculated from mass flux measurements. This means that an average time of a small single bubble passing through the microchannel was within about 0.2 s. Values of largest Lyapunov exponent shown in Table 1 are many times larger than average time of one bubble passage through microchannel. This suggests that process of stability loss does not only depend on the loss of two-phase flow stability inside the microchannel. Rather, it was connected with the behaviour of entire system, consisting of water supply system and microchannels. Changes of behaviours of entire system (Table 1) occur in time duration larger than changes occurring in two-phase flow inside the microchannel which was about 0.2 s.

In Fig. 8, the part of trajectories whose length corresponds to time of loss of stability of the system is marked by continuous bold lines. These lines contain such a number of points which is adequate to number of samples occurring in the time of stability loss of the system. In the last row of Table 1, the ratio of time of stability loss to time duration of entire cycle is listed. Note that Case 3 is the most stable boiling mode while Case 1b is the most unstable boiling mode. This is the reason why we can conclude that the system behaviour of Case 3 is close to periodic.

4. Discussion on mechanisms of oscillations

In this section, we will discuss the mechanisms on the appearance of oscillation phenomena in flow boiling in heated microchannels. It should be pointed out that heat flux supplied to the microchannels was constant but heat flux absorbed by boiling liquid q_{boil} might change during the flow boiling process. These changes in the absorbed

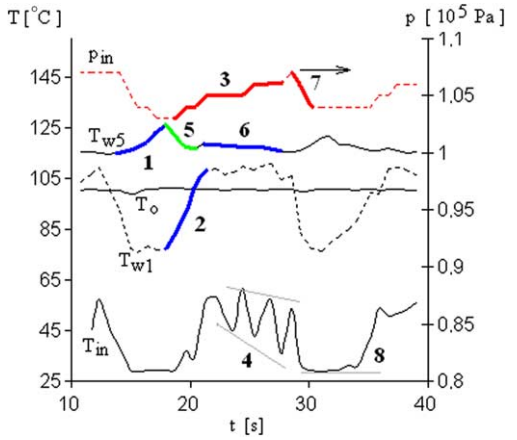

Fig. 9. Temporal variations of temperatures and pressure in liquid/two-phase alternating flow for Case 1a: $q = 13.5$ W/cm^2 and $m = 14.6$ g/cm^2 s, 1—The increase in the heating surface temperature during the liquid flow at the end of microchannels, 2—the increase in the heating surface temperature during the bubbly flow at the beginning of microchannels, 3—the increase in inlet liquid pressure during the bubbly flow, 4—inlet liquid temperature oscillations during the bubbly flow (increase of amplitude of oscillations), 5—the decrease in the heating surface temperature during the beginning stage of bubbly flow, 6—the slow decrease in the heating surface temperature during the bubbly flow, 7—the decrease in inlet pressure at the beginning of liquid-phase flow, 8—the minimum value of inlet liquid temperature.

heat flux resulted in the changes of temperature along the heating surface as shown in Fig. 2. For flow boiling in microchannels, the relation between mass flux $m(t)$ and heat flux q_{boil} determines the behaviors of the two-phase flow inside the channels.

In the following, we will discuss in detail the processes occurring during the oscillations for the four cases under consideration. In order to carry out a detailed analysis of temperature and pressure changes in the four cases under consideration, the enlarged part of data presented in Fig. 2 are shown in Figs. 9–12 respectively.

4.1. Case 1a

When the water flowed through the heated microchannels, the temperature of heated surface T_{w5} gradually increased (Fig. 9 "1") in time and in the flow direction. The highest surface temperature, T_{w5} occurred near the end of microchannel. In this time period, the temperature T_{w1} was constant because this part of heating surface was in contact with the cold inlet water. Boiling began at the end of the channel where the temperature reached the maximum value. The bubble growth at the end of the microchannel blocked the

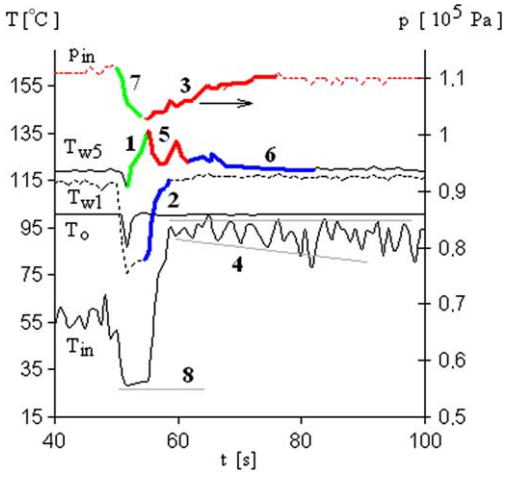

Fig. 10. Temporal variations of temperatures and pressure in liquid/two-phase alternating flow for Case 1b: $q = 16.6$ W/cm^2 and $m = 12.7$ g/cm^2 s. 1—The increase in the heating surface temperature during the liquid flow at the end of microchannels, 2—the increase in the heating surface temperature during the bubbly flow at the beginning of microchannels, 3—the increase in inlet liquid pressure during the bubbly flow, 4—inlet liquid temperature oscillations during the bubbly flow (increase of amplitude of oscillations), 5—the decrease in the heating surface temperature during the beginning stage of bubbly flow (decrease in amplitude of oscillations), 6—the slow decrease in the heating surface temperature during the bubbly flow, 7—the decrease in inlet pressure at the beginning of liquid flow, 8—the minimum value of inlet liquid temperature.

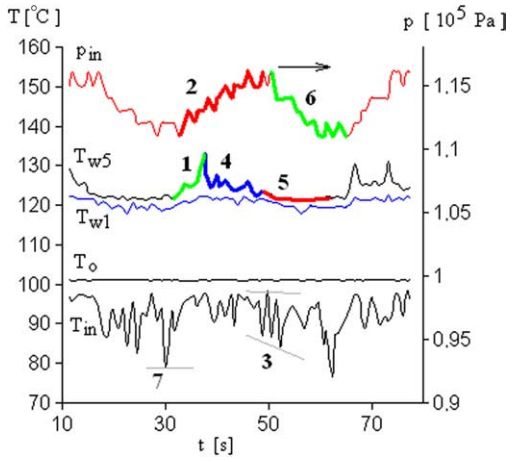

Fig. 11. Temporal variations of temperatures and pressure in continuous two-phase flow for Case 2: $q = 18.8$ W/cm^2 and $m = 11.9$ g/cm^2 s. 1—The increase in the heating surface temperature during the unstable vapour core flow at the end of microchannels, 2—the increase in inlet liquid pressure during the unstable vapour core flow, 3—inlet liquid temperature oscillations (increase in amplitude of oscillations), 4—the decrease in the heating surface temperature (decrease in amplitude of oscillations), 5—the slow decrease in the heating surface temperature during the stable vapour core flow, 7—the minimum value of inlet liquid temperature.

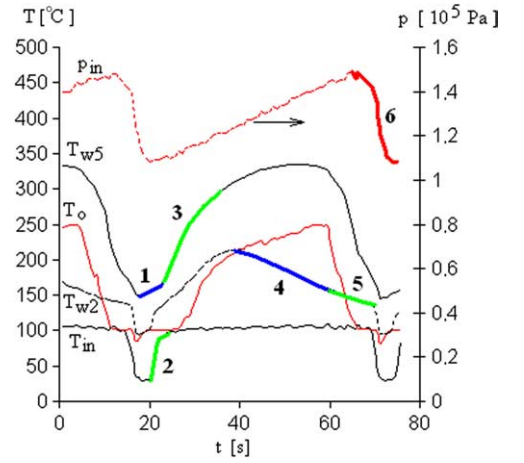

Fig. 12. Temporal variations of temperatures and pressure in liquid/two-phase/vapor alternating flow for Case 3: $q = 22.6$ W/cm^2 and $m = 11.2$ g/cm^2 s. 1—The increase in the heating surface temperature during the liquid flow, 2—the increase in inlet liquid temperature during the bubbly flow, 3—the increase in the heating surface temperature during the two-phase flow, 4—the decrease in the heating surface temperature during the vapour-phase flow, 5—decrease in the heating surface temperature during the two-phase flow, 6—the increase in inlet liquid pressure during the two-phase flow.

incoming flow, so temperature in the rest of the channel increased rapidly (Fig. 9 "2"). This resulted in spreading boiling to the entire channel and two-phase flow appeared in the channel. At the same time the temperature at the end of microchannels decreased rapidly (Fig. 9 "5").

During two-phase flow period, the growing bubbles blocked the channel and the inlet pressure p_{in} gradually increased (Fig. 9 "3"). This was accompanied by an increase in amplitude of inlet liquid temperature fluctuation (Fig. 9 "4"). The mechanism of increase in the amplitude of inlet liquid temperature fluctuation can be explained as follows: the generation of bubbles inside the microchannel blocked the flow of inlet water. This led to a decrease in mass flux, causing an increase in the inlet liquid temperature. But the process of blocking channel by bubbles also caused an increase in the inlet liquid pressure (Fig. 9 "3") and finally the mass flux increased—the blocking bubbles were partially removed from microchannel and the inlet liquid temperature decreased. When the level of mass flux (depending on the level of inlet pressure) was not large enough to decrease the heating surface temperature, then the temperature of heating surface at the channel began to increase slightly, causing the increase in boiling intensity. The bubbles started blocking the microchannel again. The process repeated itself until the level of inlet pressure was large enough to stop boiling inside the microchannel. This happened when inlet pressure reached the maximum value. The higher pressure caused the higher mass flux, therefore the minimum value of temperature of inlet liquid in subsequent cycles decreased, leading to an increase in the amplitude of oscillations (Fig. 9 "4").

During the oscillations of inlet liquid temperature, the temperature of heating surface at the end of channel gradually decreased (Fig. 9 "6"). This caused the decrease of boiling intensity in this part of channel as well. The bubbles stopped blocking the flow in the microchannel outlet, therefore bubbles from the rest of microchannel could move easier to downstream, and cold water could flow easier into the microchannel. Finally, boiling at the entire length of microchannel disappeared. Boiling in the microchannel stopped because temperature of heating surface decreased and because the inlet liquid temperature during the oscillation reached the minimum value (Fig. 9 "8"). This process resulted in the decrease of inlet pressure p_{in} (Fig. 9 "7"). When liquid flow appeared in the microchannel, the temperature of heating surface at the end of channel started to increase gradually and the process repeated itself.

The temperature at the end of microchannels T_{w5} decreased (Fig. 9 "5") when the temperature at the beginning sections of microchannels T_{w1} and inlet liquid temperature T_{in} increased (Fig. 9 "2"). Therefore, the correlation coefficients for pairs of time series (T_{in}, T_{w5}) and (T_{w1}, T_{w5}), as shown in Figs. 3 and 4 respectively, have a negative values. It reached zero value near measurement point 4. In this case, the changes in wall temperature were independent of the inlet liquid temperature. From the physical point of view, this means that the changes in wall temperature generated by nucleation process were independent of the inlet liquid temperature changes for the case under consideration.

Trajectories on attractors shown in Figs. 6a, 7a, and 8a in recurrent cycles do not lie on the same path. These changes occur because of inrecurrent time periods between subsequent cycles of oscillations. One of the reasons for appearance of these time periods changes is a stochastic characteristics of nucleation process. Points of attractor in the area 1 in Fig. 6a are created by temperature changes during the nucleation disappearance. The area 2 in Fig. 6a contains points created during the beginning of boiling, and the area 3 in Fig. 6a contains points created from temperature changes during the two-phase flow. Inrecurrent locations of trajectories in subsequent cycles are also visible in Fig. 7a. The points of attractor in area 1 in Fig. 7a is created by pressure fluctuation during the two-phase flow period.

A low correlation dimension of attractor (2.25) for Case 1a obtained from temperature fluctuation (see Table 1) shows that the thermal interaction between the heating surface and liquid flow can be described by a low dimensional model with 2 degree of freedom e.g. $m(t)$ and $q_{boil}(t)$. The correlation dimension of attractor from the pressure fluctuation has the similar dimension. Thus, we can conclude that the process in Case 1a has the deterministic chaos characteristics.

4.2. Case 1b

The mechanism of appearance of the oscillations in Case 1b seems to be similar to that observed in Case 1a. Boiling began not at the end of the channel but inside the microchannel, because temperatures T_{w3} and T_{w4} reached the maximum values [18] during the recurrent cycles. Since the correlation coefficients between T_{in}, T_{w1} and T_{w5} are close to zero (Figs. 3 and 4), therefore, the changes of temperature T_{w5} are independent of temperatures T_{in}, T_{w1} changes in this case.

When water flowed through the heated microchannels, the temperature of heated surface T_{w1}, T_{w5} gradually increased (Fig. 10 "1") in time. The highest surface temperature occurred near the end of microchannel, T_{w4} [18]. In this time period the temperature T_{w1} increased slowly. The bubbles growth in the microchannel blocked the incoming flow, so temperature in the rest of the channel increased rapidly (Fig. 10 "2"). This resulted in spreading the boiling to the entire channel and two-phase flow appeared in the channel.

During two-phase flow period, when the growing bubbles blocked the channel, the inlet pressure p_{in} gradually increased (Fig. 10 "3"). It was accompanied by an increase in amplitude of inlet liquid temperature fluctuation (Fig. 10 "4"). The mechanism of increase in the amplitude of fluctuation seems to be the same like in Case 1a. But because the heat flux was larger than in Case 1a, therefore the time of decrease in the inlet temperature up to the temperature of boiling disappearance was larger than in Case 1a.

During the boiling process, temperatures of the heating surface gradually decreased (Fig. 10 "6"). At the same time, the inlet pressure gradually increased (Fig. 2b "3") which resulted in the increase of mass flux. The inlet liquid temperature oscillated and its value slowly decreased (Fig. 2b "4"). The boiling in channel stopped because temperature of heating surface decreased and because the inlet liquid temperature during the oscillation reached the minimum value (Fig. 10 "8").

The area 1 in Fig. 6b contains the points created by process of nucleation disappearance, the area 2 in Fig. 6b contains points created during the beginning of the boiling and the area 3 in Fig. 6b contains points created from temperature changes during the two-phase flow. This area is more dense in comparison with the Case 1a, because the time period of two-phase flow existing in the Case 1b is longer than in Case 1a. This kind of attractor structure causes that the correlation dimension of attractor from temperature T_{w1} is 5.2 (Table 1). The correlation dimension of attractor reconstructed from inlet pressure is 5.5. The area 1 in Fig. 7b is created by pressure fluctuation during the two-phase flow. We can conclude that the process has the deterministic chaos characteristics.

4.3. Case 2

For Case 2 the correlation between the wall temperature oscillation is constant and is equal to 0.8 (see Fig. 3). This means that, the wall temperatures changes with time in the same way. This happened because heat flux was large enough to sustain the boiling on the entire length of channels. The correlation coefficients between the inlet liquid temperature and wall temperatures at the beginning part of microchannels are lower than those in Cases 1a and 1b (Fig. 4). This implies that the dynamics of inlet liquid temperature changes is somewhat different from dynamics of the wall temperature changes. This also results in the difference of correlation dimension of attractors from T_{in} ($D = 6$) and p_{in} ($D = 4.2$). These differences are caused by intensive nucleation processes occurring in the entire length of microchannels.

When the inlet liquid temperature reached the minimum value (Fig. 11 "7"), the wall temperature and pressure reached the minimum value as well. In this case, the volume of vapour core inside the microchannel decreased. Because the mass flux is low, the temperature of the heating surface started to increase (Fig. 11 "1"), causing the increase of the evaporation intensity. The volume of vapour inside the microchannel increased and vapour core started to block the microchannel and decreased the mass flux, causing an increase in the heating surface temperature (Fig. 11 "1") and inlet pressure (Fig. 11 "2"). During this process the heating surface temperature oscillated at the channel outlet (Fig. 11 "4"). Finally, the increase in inlet pressure (Fig. 11 "2") led to an increase in mass flux. Because the heat flux supplied to the heating surface was not large enough to increase the heating surface temperature at high mass flux, the temperature of heating surface decreases (Fig. 11 "5"). This caused the intensity of evaporation to decrease as well, that led to decreasing the volume of vapour inside the microchannel. The pressure (Fig. 11 "6"), surface temperatures (Fig. 11 "5"), as well as the mean inlet liquid temperature (Fig. 11 "3") decreased. During the pressure decrease (Fig. 11 "6") the oscillations of the inlet liquid temperature appeared (Fig. 11 "3"). When the temperature of heating surface (Fig. 11 "7") and pressure reached the minimum values, the vapour core stabilised and the process repeated itself.

The mechanism of appearance of heating surface temperature fluctuation during the increase in inlet pressure can be explained as follows: During the inlet pressure increase (Fig. 11 "2") the mass flux increased as well, causing decrease of evaporation intensity and the decrease in heating surface temperature. Due to intensive evaporation the volume of vapour core inside the microchannel increased and blocked the flow of inlet water. Consequently, mass flux decreased. The intensity of evaporation increased and temperature of heating surface increased. Because the moving vapor core blocked the microchannel the inlet pressure increases causing the increase of mass flux. As a result the heating surface temperature decreased and the process repeated itself, at the higher level of pressure (pressure fluctuation in Fig. 11 "2"). This kind of fluctuation disappeared when the mass flux was large enough to stop the process of increase in the heating surface temperature.

The mechanism of inlet liquid temperature fluctuation during the decrease in inlet pressure can be explained as follows: During the inlet pressure decreased (Fig. 11 "6") the mass flux decreased as well, causing the increase of evaporation intensity. The volume of vapour core inside the microchannel increased and blocked the flow of inlet water. But the process of blocking the channel by the moving vapor core caused also a slight increase in the inlet liquid pressure (pressure fluctuation in Fig. 11 "6") and finally, the mass flux increases—the intensity of boiling decreased and the vapor core stabilized causing further decrease in inlet pressure and the process repeated itself.

It should be noted that changes of location of attractor trajectories visible in Figs. 6 and 7 are caused by changes of dynamics of two-phase flow in the microchannels. The process has the deterministic chaos characteristics.

4.4. Case 3

For this case, the correlation between the measurements of heating surface temperature at different points is high as seen from Fig. 3. This means that temperatures at different parts of heating surface changed in the same way. As shown in Fig. 4, the correlation between the inlet liquid temperature and heating surface temperatures reached the minimum value at the measurement point T_{w3}, but the level of correlation was still high.

When the liquid flow appeared in the channel, the inlet liquid temperature and heating surface temperature decreased. The outlet liquid temperature started to increase (Fig. 12 "1"). The highest temperature of heating surface occurred at the end of the channel. When boiling started at the end of channel, it spreaded rapidly to the entire channel. Because the heat flux was high in Case 3, a vapour core was formed inside the channel. Two-phase flow at the beginning of the microchannel blocked the inlet flow of water. The temperature of inlet water rapidly increased (Fig. 12 "2"). Due to high heat flux, the heating surface temperature still increased, causing the appear-

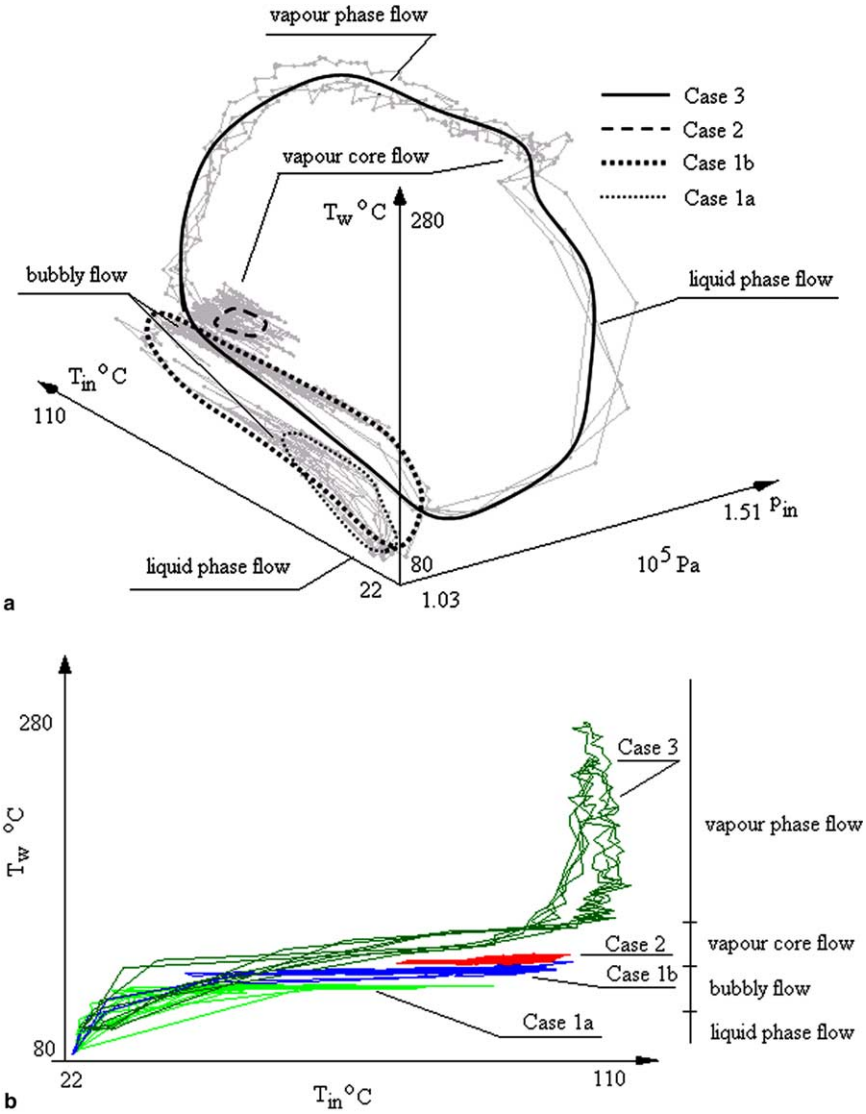

Fig. 13. Map of appearance of boiling modes in the space of p_{in}, T_{in}, T_w. (a) Schematic drawing of microchannels system cycles in 3D state-space (p_{in}, T_{in}, T_w), and (b) map of boiling modes in 2D state-space of T_{in}, T_w.

ance of the vapour-phase flow inside the microchannel (Fig. 12 "3"). In this flow pattern, the temperature of heating surface at the beginning of microchannels started to drop because of intensive liquid evaporation (Fig. 12 "4"). Because the heat supplied to the beginning part of microchannels was insufficient to sustain the intensive evaporation, the temperature T_{w2} and vapour-phase flow disappeared and two-phase flow appeared (Fig. 12 "5"). Because of the high inlet pressure, the mass flux was also high. Therefore, the temperature of heating surface decreased, causing the disappearance of boiling. This resulted in the decrease in inlet pressure p_{in} (Fig. 12 "6"). The temperature of heating surface started to increase and a new cycle began again.

The correlation dimension of attractor from the heating surface temperature is about 1.1 while the correlation dimension of attractor from inlet pressure fluctuations is about 1. Points of attractor in the area 1 in Fig. 6d are created by temperature changes during the nucleation disappearance. The area 2 in Fig. 6d contains points created during the beginning of boiling.

The above discussion can be summarized in Fig. 13. Fig. 13a shows the schematic drawing of microchannels system trajectories in state-space variables p_{in}, T_{in}, T_w for the four cases under consideration. Grey points and lines in the graph represent the real location of system trajectories. Black lines schematically show the average changes of (p_{in}, T_{in}, T_w) during the cyclic changes of system. It is noted that the dynamics of oscillations and location of each cycle depends on the value of heat flux supplied to the system (each cycle in Fig. 13 has been created for different heat flux). But mechanism of appearance of cycles seems to be the same for all four cases under consideration. During the liquid flow period, the average temperature of the heating surface T_w increases and boiling begins at the end parts of channels where the temperature is the highest. The two-phase flow in microchannel controls the mass flux and works as a negative feedback for the process of increasing wall temperature. Because of intensive boiling inside the microchannel, the heating surface temperature starts to decrease and finally the boiling process stops.

Fig. 13b shows the map of appearance of four kinds of flow in microchannels system in state-space (T_{in}, T_w). On the right side of the graph, the ranges of average wall temperature T_w where the different kinds of flow appear in microchannels are indicated. In Table 1 the average wall temperature characteristics for the four cases under consideration are also presented. Depending on the heating surface and liquid temperature, the following four kinds of flow patterns may occur in a microchannel: liquid-phase flow, bubbly flow, vapour core flow and vapour-phase flow. The liquid-phase flow is characterised by the lowest average heating surface temperature while the vapour-phase flow is characterised by the highest heating surface temperature. When the heat flux supplied to the microchannel is large enough to increase the temperature of heating surface to an appropriate level, one of the boiling modes as shown in Fig. 13b, will appear in the microchannel. The vapour core flow at two different liquid pressures are depicted in Fig. 13a. In Case 3 during the decrease in the heating surface temperature it has been observed: the vapour-phase flow, vapour core flow and liquid-phase flow. The bubbly flow was not observed. This happened because during the destabilization of vapour core the mass flux was large enough to decrease the heating surface temperature to the value which is characteristic for liquid-phase flow.

It should be noted that the map of occurrence of four boiling modes, presented in Fig. 13, is by no means complete because we have no knowledge about (i) the transition between the considered modes, and (ii) the sensitivity of considered boiling modes to the changes of heat and mass fluxes supplied to the system. Therefore, further experimental investigations are necessary to better understand the dynamics of heat and mass transfer in flow boiling in a microchannel.

5. Concluding remarks

In this paper, we have carried out non-linear analyses for the four unstable boiling modes in microchannels observed by Wu and Cheng [18]. The results of these analyses show that oscillations of temperature and pressure occurring in flow boiling in microchannel have deterministic chaos characteristics. The following conclusions are obtained:

1. The appearance of deterministic chaos in cases under consideration is confirmed by positive values of largest Lyapunov exponent. The system is more predictable in Case 3 and more chaotic in Cases 2 and 1b. In Case 1b the large number of points of attractor is located in area "3" (Fig. 6b). This area is created by temperature fluctuation in bubbly flow, therefore the level of chaos obtained in this case is connected rather with the bubbly flow than with oscillations of the entire system.
2. The reconstruction of attractors from temperature and pressure indicates that, the trajectories of attractors are located inside the torus in 3D space for all cases under consideration. The reconstruction of the system trajectory in the state-space (T_{in}, p_{in}, T_w) shows that the trajectories are located also inside the torus like trajectories obtained using the delay time method. This suggests that parameters (T_{in}, p_{in}, T_w) are crucial to describing the system behaviors in microchannel system.
3. It has been found that when the heat flux is increased, the number of independent variables controlling the

behavior of system increases as well. For a low heat flux equal to 13.5 W/cm^2 (Case 1a), the number of independent variables is equal to 3. While the heat flux is increased to 18.8 W/cm^2 (Case 2), then the number of independent variables reaches value equal to 6, which is characteristic for a vapor core flow. Finally, the number of independent variables describing the system decreases to value equal to 1, when the heat flux reaches 22.6 W/cm^2 (Case 3). The calculation of correlation dimension also shows that in Cases 1a, 1b, 3 the changes of T_{in} and p_{in} are controlled by the same set of physical parameters. In Case 2 the sets of independent physical parameters describing the changes of T_{in} and p_{in} are different.

4. Values of the largest Lyapunov exponent shown in Table 1 are many times larger than average time of one bubble passage through microchannel. This suggests that process of stability loss is connected with the behavior of entire system, consisting of water supply system and microchannels.
5. For all cases under consideration the temperature changes of the heating surface at measurement points T_{w1}, T_{w2}, T_{w3} are correlated in the same way. The qualitative differences between temperature change characteristics occurring near the end of the microchannel in Cases 1a, 1b and the temperature changes in Cases 2, 3 have been identified.
6. A detailed analysis of temperature and pressure changes show that for flow boiling in microchannels, the relation between the mass flux $m(t)$ and heat flux q_{boil} determines the behaviors of the two-phase flow inside the channels. In general the mechanism of oscillations in boiling in microchannels is as follows: cycles start when the temperature of the heating surface begins to increase and the boiling begins to appear in the microchannel. The appearance of vapor inside the microchannels blocks the liquid flowing into the microchannel. Therefore, the inlet liquid pressure increases and mass flux increases as well. When the heat flux q_{boil} is not large enough the boiling inside the microchannels with high mass flux leads to decreasing in the heating surface temperature, and consequently to the decrease of boiling intensity (Case 2) or boiling disappearance (Cases 1a, 1b, 3). The bubbles stop blocking the microchannel and inlet pressure decreases, where upon the cycle repeats itself.

References

[1] H. Yuncu, O.T. Yildirim, S. Kakac, Two-phase flow instabilities in a horizontal single boiling channel, Appl. Sci. Res. 48 (1991) 83–104.

[2] Y. Ding, S. Kakac, X.J. Chen, Dynamic instability of boiling two-phase flow in a single horizontal channel, Exp. Thermal Fluid Sci. 11 (1995) 327–342.

[3] Q. Wang, X.J. Chen, S. Kakac, Y. Ding, Boiling onset oscillation: a new type of dynamic instability in a forced convection upflow boiling system, Int. J. Heat Fluid Flow 17 (4) (1996) 418–423.

[4] M. Xiao, X.J. Chen, M.Y. Zhang, T.N. Veziroglu, S. Kakac, A multivariable liner investigation of two-phase flow instabilities in parallel boiling channels under high pressure, Int. J. Multiphase Flow 19 (1) (1993) 65–77.

[5] J.M. Kim, S.Y. Lee, Experimental observation of flow instability in a semi-closed two-phase natural circulation loop, Nucl. Eng. Des. 196 (2000) 359–367.

[6] V. Heinzel, J. Holzinger, M. Simon, Fluid oscillation in flat plat boiling water collectors, Solar Energy 59 (1997) 43–48.

[7] M.B. Bowers, I. Mudawar, High flux boiling in low flow rate, low pressure drop mini-channel and microchannel heat sinks, Int. J. Heat Mass Transfer 37 (2) (1994) 321–332.

[8] W. Qu, I. Mudawar, Prediction and measurements of incipient boiling heat flux in microchannel heat sinks, Int. J. Heat Mass Transfer 45 (2002) 3933–3945.

[9] X.F. Peng, H.Y. Hu, B.X. Wang, Boiling nucleation during liquid flow in microchannels, Int. J. Heat Mass Transfer 41 (1) (1998) 101–106.

[10] L. Jiang, M. Wong, Y. Zohar, Forced convection boiling in a microchannels heat sink, J. Microelectromech. Syst. 10 (1) (2001) 80–87.

[11] L. Zhang, J.M. Koo, L. Jiang, M. Asheghi, K.E. Goodson, J.G. Santiago, Measurements and modeling of two-phase flow in microchannels with nearly constant heat flux boundary conditions, J. Microelectromech. Syst. 11 (1) (2002) 12–17.

[12] G. Hetsroni, A. Mosyak, Z. Segal, Nonuniform temperature distribution in electronic devices cooled by flow in parallel microchannels, IEEE Trans. Components Packag. Technol. 24 (1) (2001) 17–23.

[13] G. Hetsroni, A. Mosyak, Z. Segal, G. Ziskind, A uniform temperature heat sink for cooling of electronic devices, Int. J. Heat Mass Transfer 45 (2002) 3275–3286.

[14] H.Y. Wu, P. Cheng, Visualization and measurements of periodic boiling in silicon microchannels, Int. J. Heat Mass Transfer 46 (2003) 2603–2614.

[15] H.Y. Wu, P. Cheng, Liquid/two-phase/vapor alternating flow during boiling in microchannels at high heat flux, Int. Commun. Heat Mass Transfer 30 (3) (2003) 295–302.

[16] H.Y. Wu, P. Cheng, Two large-amplitude/long-period oscillating boiling modes in silicon microchannels, in: Proceedings of the First International Conference on Microchannels and Minichannels, ASME, Rochester, NY, 2003, pp. 629–633.

[17] H.Y. Wu, P. Cheng, Three boiling instability modes in silicon microchannels, in: Proceedings of ASME Summer Heat Transfer Conference, HT2003-47463, Nevada, Las Vegas, 2003.

[18] H.Y. Wu, P. Cheng, Boiling instability in parallel silicon microchannels at different heat flux, Int. J. Heat Mass Transfer 47 (2004) 3631–3641.

[19] H.G. Schuster, Deterministic Chaos An Introduction, Physik-Verlag GmbH, Weinheim, 1984.
[20] A. Wolf, J.B. Swift, H.L. Swinney, J.A. Vastano, Determining Lyapunov exponent from a time series, Phisica-D 16 (1985) 285–317.
[21] P. Grassberger, I. Procaccis, Measuring the strangeness of strange attractors, Physica D 9 (1985) 189–208.
[22] J. Awrejcewicz, R. Mosdorf, Analiza numeryczna wybranych zagadnie dynamiki chaotycznej, WNT, Warsaw, 2003 (in Polish).